International Journal of
Molecular Sciences

MDPI

Article

Associations of *Lactobacillus helveticus* PP0208 and Its Derivatives with Allergic Rhinitis-Related Phenotypes, Immune Parameters, and Gut Microbiota in OVA-Challenged Mice

Qingtai Meng [1,2], Meng Yuan [1,2], Chongyao Xue [1,2], Mingyang Ding [1,2], Xinhang Li [1,2] and Yong Fang [1,2,*]

[1] Department of Microbiology, School of Basic Medical Sciences, Harbin Medical University, No. 157 Baojian Road, Nangang District, Harbin 150081, China
[2] Heilongjiang Province Key Laboratory of Immunity & Infection, Harbin 150081, China
* Correspondence: yong.fang@ems.hrbmu.edu.cn

Abstract

Allergic rhinitis (AR) is a prevalent IgE-mediated inflammatory disease driven by Th2-skewed immune dysregulation, and gut-immune-targeted interventions, including probiotic supplementation, have attracted growing attention as adjunctive strategies. This study characterized the phenotypic, immune, microbial, and metabolic associations of *Lactobacillus helveticus* PP0208 and its derivatives—live bacteria (Lh-PP0208), heat-killed PP0208 (Lh-PP0208-HK), and PP0208-derived extracellular vesicles (Lh-PP0208-EVs)—in an OVA-challenged AR mouse model. Supplementation with *L. helveticus* PP0208 and its derivatives was associated with alleviated nasal allergic symptoms, reduced splenic hypertrophy, decreased nasal mucosal eosinophil and mast cell infiltration, and mitigated pulmonary and colonic mucosal structural changes. The intervention was associated with a Th1/Th2-related cytokine profile (elevated IFN-γ and IL-10; reduced IL-4 and IgE) and an increased proportion of splenic $CD4^+CD25^+FOXP3^+$ Treg cells. 16S rRNA gene amplicon sequencing revealed that *L. helveticus* PP0208 and its derivatives were associated with shifts in gut microbial community structure, microbial co-occurrence networks, and partial increases in several genera depleted under OVA challenge, including *Limosilactobacillus* and *Ligilactobacillus*. Untargeted metabolomics further revealed associated shifts in gut metabolic profiles, involving amino acid, SCFA-related and immune-related pathways. Integrated multi-omics correlation analysis revealed associations between differential gut bacteria, metabolite features and allergic symptoms. Collectively, *L. helveticus* PP0208 and its derivatives were associated with reduced allergic symptoms, a shift toward a Th1/Treg-oriented cytokine profile, partial shifts toward control-like gut-microbiota community structures, and altered fecal metabolic profiles enriched in SCFA-related and amino-acid pathways. These correlative findings provide preliminary evidence for strain-derived multi-form interventions against allergic inflammation.

Keywords: allergic rhinitis; *Lactobacillus helveticus*; gut microbiota; metabolites; immune modulation

Check for updates

Academic Editors: Joohyun Nam and Kyu-Sup Cho

Received: 8 October 2026
Revised: 3 November 2026
Accepted: 16 November 2026
Published: 24 November 2026

Copyright: © 2026 by the authors. Licensee MDPI, Basel, Switzerland. This article is an open access article distributed under the terms and conditions of the Creative Commons Attribution (CC BY) license.

1. Introduction

Allergic rhinitis (AR) is a highly prevalent chronic inflammatory disease of the upper respiratory tract, driven by IgE-mediated Th2-skewed immune responses to environmental allergens [1,2]. With increasing urbanization and allergen exposure, the global prevalence of AR continues to rise, imposing substantial quality-of-life impairment and economic burden [3]. Current management relies on intranasal corticosteroids, antihistamines,

leukotriene receptor antagonists, and allergen immunotherapy [4]. However, pharmacotherapy only provides symptomatic relief; a subset of patients responds poorly, and immunotherapy is limited by long treatment courses and adherence requirements [5–8]. There is therefore a recognized need for safe, adjunctive interventions that sustainably modulate immune balance in AR.

Gut microbiota has emerged as a key regulator of immune development and tolerance, and perturbations in early-life microbiota are associated with increased risk of allergic disease [9–11]. Probiotic supplementation has therefore been investigated as an approach for AR. Meta-analyses and randomized trials have reported that selected strains (e.g., *L. rhamnosus*, *L. plantarum*, *L. paracasei*) can reduce nasal symptom scores and enhance anti-inflammatory cytokines in AR, but results remain strain-specific and heterogeneous: efficacy varies across strains, study designs, and dosing regimens, and a substantial proportion of trials report no significant benefit [12–14]. This heterogeneity underscores that the anti-allergic activity of probiotics cannot be generalized across species or even strains, and that novel strains with well-characterized immunomodulatory profiles continue to be needed.

A further limitation of live probiotics is their dependence on viable colonization: viability during storage and gastrointestinal transit is variable, and viable bacteria carry theoretical risks in immunocompromised populations. These concerns have driven interest in postbiotics—non-viable bacterial preparations or their derivatives—as safer, more stable alternatives. Heat-killed bacteria retain cell-wall and cytoplasmic immunomodulatory components without requiring viability [15]. Extracellular vesicles (EVs)—nanosized membrane particles released by bacteria—represent an even more defined cell-free format: they carry proteins, lipids, and nucleic acids that mediate host–microbe communication, and bacterial EVs have been shown to modulate intestinal immunity in colitis and infection models [16]. However, EV-based interventions in allergic rhinitis remain largely unexplored.

Against this background, three unresolved questions motivated the present study. First, although postbiotics and bacterial EVs are emerging as safer alternatives to live probiotics, few AR studies have examined non-viable or EV preparations in parallel with the live parent strain in the same allergic model, and it remained unclear whether each non-viable preparation could, within its own dosing metric, be associated with alleviation of allergic inflammation. Second, although gut microbiota and fecal metabolites are implicated in allergic inflammation, few AR studies have integrated 16S rRNA sequencing with untargeted metabolomics to characterize the microbial and metabolic shifts that accompany probiotic intervention. Third, the anti-allergic activity of *Lactobacillus helveticus* PP0208 has not been examined in AR.

In the present study, an OVA-challenged AR mouse model was used to test whether *L. helveticus* PP0208 and its derivatives would be individually associated with alleviation of allergic inflammation under their own dosing regimen, and whether such effects would be accompanied by shifts in gut microbiota and fecal metabolome alongside changes in immune parameters. We administered the three preparations in parallel alongside the OVA model group and alum-only (adjuvant-only) non-allergic control group, and combined allergic behavioral, histological and immunological phenotyping with 16S rRNA gene amplicon sequencing and untargeted fecal metabolomics on a balanced subset of animals. Given the different dose metrics used for the three preparations (CFU, TFU, and EV protein mass), this parallel design assesses associations with phenotype rather than direct quantitative efficacy comparison among preparations. This approach provides preliminary evidence for cell-free probiotic strategies against AR and a framework for future mechanistic studies.

2. Results

2.1. Phenotypic Alterations Associated with L. helveticus PP0208 and Its Derivatives in OVA-Challenged AR Mice

To explore the anti-allergic activities of live *L. helveticus* PP0208 (Lh-PP0208), heat-killed Lh-PP0208 (Lh-PP0208-HK), and Lh-PP0208-derived extracellular vesicles (Lh-PP0208-EVs), we isolated the Lh-PP0208 strain and prepared bacterial EVs following the workflow illustrated in Figure 1A. The uninoculated MRS-medium control and purified EVs were characterized by TEM and NTA, as shown in Figure 1B. In contrast to the purified EV preparations, no vesicular structures were visualized in pure MRS medium after ultracentrifugation and purification, ruling out potential interference from medium-derived vesicles. An OVA-challenged allergic rhinitis (AR) mouse model was established following the experimental timeline outlined in Figure 1C. Body weight was recorded throughout the OVA challenge phase. No marked growth suppression was observed across all groups (Figure 1D), suggesting that these oral interventions exerted no detectable adverse toxic effects on mouse growth. Allergic behavioral symptoms, including nose-rubbing frequency and sneezing events within 10 min, were recorded immediately after the final intranasal OVA challenge. As displayed in Figure 1E,F, the OVA group exhibited elevated nose-rubbing and sneezing counts compared with the Control group ($p < 0.001$). Under the experimental conditions, administration of *L. helveticus* PP0208 and its derivatives was associated with significantly ameliorated allergic behaviors compared with the OVA group. Direct quantitative comparison of their efficacy is precluded by the different dose metrics. Spleen morphology and spleen index were further analyzed to evaluate systemic immune activation. The spleen showed obvious splenomegaly and increased index in OVA-challenged mice relative to the Control group (Figure 1G,H, $p < 0.001$). Supplementation with Lh-PP0208, Lh-PP0208-HK or Lh-PP0208-EVs was associated with diminished OVA-challenged splenic enlargement and a lower spleen index. Cytological analysis of BALF was performed to characterize infiltrated inflammatory cells (Figure 1I). Differential cell counting demonstrated that eosinophils and lymphocytes were increased in the OVA group, whereas macrophage proportion decreased (Figure 1J–L, $p < 0.001$). In contrast, intervention with Lh-PP0208, Lh-PP0208-HK or Lh-PP0208-EVs was accompanied by reduced eosinophil and lymphocyte infiltration, and increased proportions of macrophages in BALF.

Collectively, these observations indicated that intervention with Lh-PP0208 and its derivatives was associated with ameliorated allergic symptoms and reduced local inflammatory cell infiltration.

2.2. Immune- and Mucosal-Tissue-Related Changes Associated with L. helveticus PP0208 and Its Derivatives in OVA-Challenged AR Mice

To characterize the immune phenotype associated with the anti-allergic effects of *L. helveticus* PP0208 and its derivatives, the proportion of splenic $CD4^+CD25^+FOXP3^+$ Tregs was detected via flow cytometry (Figure 2A,B). Compared with the Control group, the frequency of $CD4^+CD25^+FOXP3^+$ Tregs was reduced in the OVA group ($p < 0.001$). Treatment with Lh-PP0208, Lh-PP0208-HK or Lh-PP0208-EVs was accompanied by a higher percentage of Tregs, a pattern consistent with an immune-tolerant phenotype.

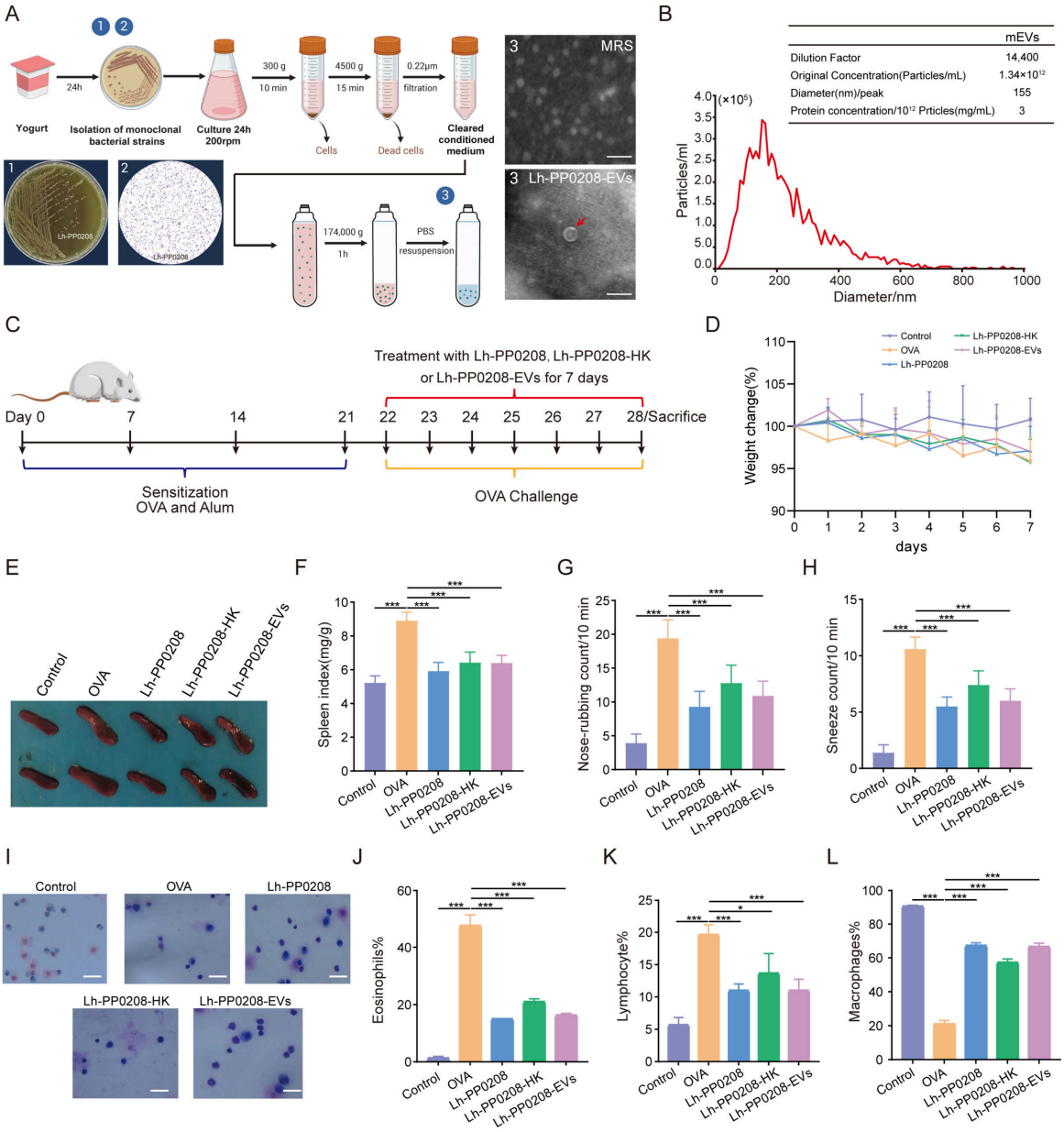

Figure 1. Phenotypic alterations associated with *L. helveticus* PP0208 and its derivatives in OVA-challenged AR mice. (**A**) Workflow for isolation of monoclonal *L. helveticus* PP0208 strains and preparation of bacterial EVs. 1: colony morphology on agar plate; 2: Gram-staining image; 3: TEM observation of purified MRS and EVs. A scale bar = 200 nm is shown in the figure. The particle size distribution and quantitative parameters of EVs are also displayed. (**B**) Representative TEM image of purified Lh-PP0208-EVs (red arrow indicates EV particle), together with NTA profile of EVs. (**C**) Schematic timeline of the murine allergic rhinitis (AR) model establishment, sensitization, OVA challenge, and intervention with live Lh-PP0208, Lh-PP0208-HK and Lh-PP0208-EVs. The Control group received i.p. saline containing 2 mg aluminum hydroxide adjuvant without OVA (alum-only non-allergic control), followed by intranasal saline and oral saline. (**D**) Dynamic changes in body weight of mice during OVA challenge and treatment. (**E**,**F**) The frequency of nose-rubbing (**E**) and sneezing (**F**) behaviors recorded for 10 min immediately after the final intranasal OVA challenge. (**G**) Representative photographs of spleens harvested from each group. (**H**) Quantitative analysis of spleen index in different groups. (**I**) Representative cytological images of BALF inflammatory cells. A scale bar = 20 μm is shown in the figure. (**J**–**L**) Quantification of the proportions of eosinophils (**J**), lymphocytes (**K**), and macrophages (**L**) in BALF. Data are presented as mean ± SEM. $n = 12$/group. * $p < 0.05$, *** $p < 0.001$. Created in BioRender. Meng, Q. (2026) https://BioRender.com/r3nzow2.

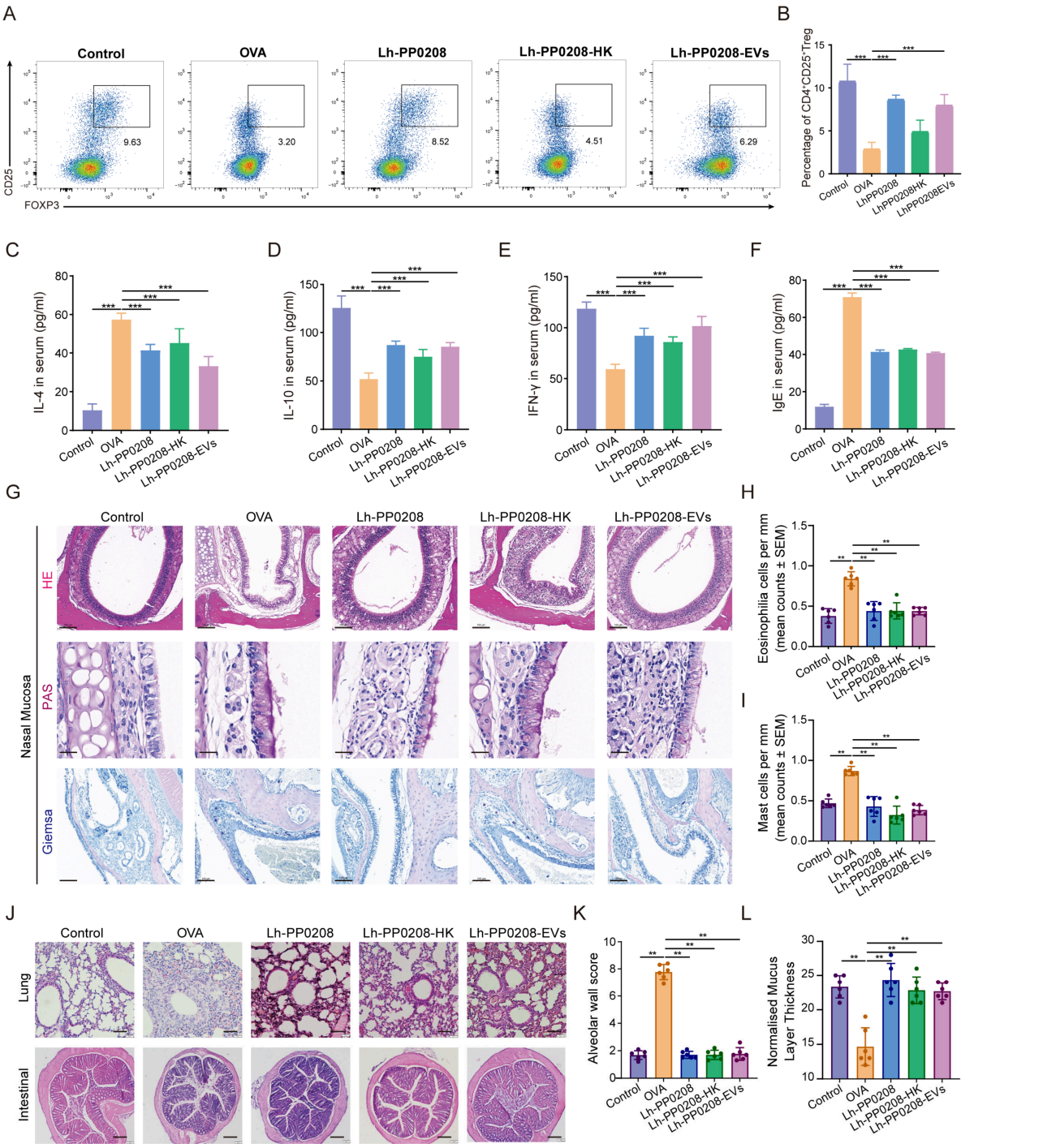

Figure 2. Immune- and mucosal-tissue-related changes associated with *L. helveticus* PP0208 and its derivatives in OVA-challenged AR mice. (**A**) Representative flow-cytometry density plots (pre-gated on $CD4^+$ lymphocytes) showing $CD4^+CD25^+FOXP3^+$ regulatory T (Treg) cells. Color gradient in the density plots indicates cell event density, with red representing the highest density and blue representing sparse events. (**B**) Statistical analysis of the proportion of $CD4^+CD25^+FOXP3^+$ Tregs. (**C**–**F**) ELISA detection of serum levels of IL-4 (**C**), IL-10 (**D**), IFN-γ (**E**) and IgE (**F**), $n = 12$/group. (**G**–**I**) Histopathological staining of nasal tissues (H&E, scale bar = 100 μm, PAS scale bar = 20 μm, Giemsa scale bar = 100 μm) and quantitative statistics of eosinophils and mast cells per millimeter of nasal epithelium. Scale bars are shown in the images, $n = 6$/group. (**J**–**L**) H&E staining of pulmonary and colonic tissues scale bar = 40 μm, followed by quantitative analysis of alveolar wall score and normalized mucosal thickness, $n = 6$/group. Data are presented as mean ± SEM. ** $p < 0.01$, *** $p < 0.001$.

Subsequently, Th1/Th2 cytokines and total IgE in serum were quantified by ELISA (Figure 2C–F). The OVA group exhibited increased concentrations of the Th2-type cytokine IL-4 and total IgE, accompanied by a decrease in the Th1 cytokine IFN-γ and anti-inflammatory cytokine IL-10 relative to the Control group ($p < 0.001$). Intervention with *L. helveticus* PP0208 and its derivatives was accompanied by diminished overproduction of IL-4 and IgE, while also being accompanied by elevated serum concentrations of IL-10 and IFN-γ. These results suggested that Lh-PP0208 and its derivatives were associated with shifts away from disrupted Th1/Th2-related cytokine balance and enhanced anti-inflammatory responses in allergic rhinitis.

We further evaluated local inflammation in nasal mucosa by histological staining (Figure 2G). H&E staining revealed inflammatory infiltration in the nasal mucosa of OVA-challenged mice. PAS staining demonstrated abundant goblet cell hyperplasia and excessive mucus secretion, and Giemsa staining identified massive infiltration of eosinophils and mast cells in the OVA group. Quantitative statistics confirmed significantly elevated densities of eosinophils and mast cells per millimeter of nasal tissue in the OVA group (Figure 2H,I). By contrast, mice receiving all three interventions showed alleviated mucosal edema, reduced inflammatory cell infiltration, suppressed goblet cell proliferation and decreased mucus production.

We next performed histological assessment of pulmonary and intestinal tissues (Figure 2J). Severe peribronchial inflammatory infiltration and thickened alveolar walls were observed in the pulmonary tissue of OVA model mice. In addition, intestinal morphological disorders and thinner mucosal layers were detected in the OVA group. Quantitative analysis showed a higher alveolar wall score and reduced normalized intestinal mucosal thickness in the OVA group (Figure 2K,L). For mice receiving Lh-PP0208, Lh-PP0208-HK or Lh-PP0208-EVs, findings were consistent with mitigated pulmonary inflammatory injury and better-preserved intestinal mucosal barrier architecture. Collectively, these data indicated that Lh-PP0208 and its derivatives were associated with ameliorated systemic allergic-like inflammation alongside shifts in adaptive immune readouts and better-preserved mucosal tissue architecture across multiple organs.

2.3. Associated Shifts in Gut Microbiota Profiles Following L. helveticus PP0208 and Its Derivatives Treatment in OVA-Challenged AR Mice

To investigate gut-microbiota-related changes associated with Lh-PP0208 and its derivatives under allergic rhinitis-like conditions, 16S rRNA gene amplicon sequencing was conducted on mouse feces. Alpha diversity of gut microbiota was evaluated with Shannon and Simpson indices (Figure 3A,B). A marked decrease in the Shannon index and an increase in the Simpson index were observed in OVA-challenged mice relative to the Control group, indicating reduced microbial diversity following OVA sensitization. Alpha-diversity indices shifted toward Control-group levels upon intervention with Lh-PP0208, Lh-PP0208-HK or Lh-PP0208-EVs. Beta-diversity analysis based on ASV profiles was conducted using PCA and PCoA (Figure 3C,D). PERMANOVA based on Bray–Curtis distances revealed a significant overall difference in gut microbiota composition among the five groups ($R^2 = 0.699$, $p = 0.001$, Table S1). PERMDISP showed no significant difference in within-group dispersion ($F = 3.21$, $p = 0.091$, Table S2), confirming that the observed differences were not driven by unequal group dispersions. Clear separation was observed between the Control and OVA groups, demonstrating that OVA sensitization and challenge induced profound shifts in the gut microbial community. Notably, samples from the Lh-PP0208, Lh-PP0208-HK and Lh-PP0208-EVs groups were separated from the OVA group and shifted toward the Control group, showing that gut microbial profiles shifted toward the Control-like state following intervention.

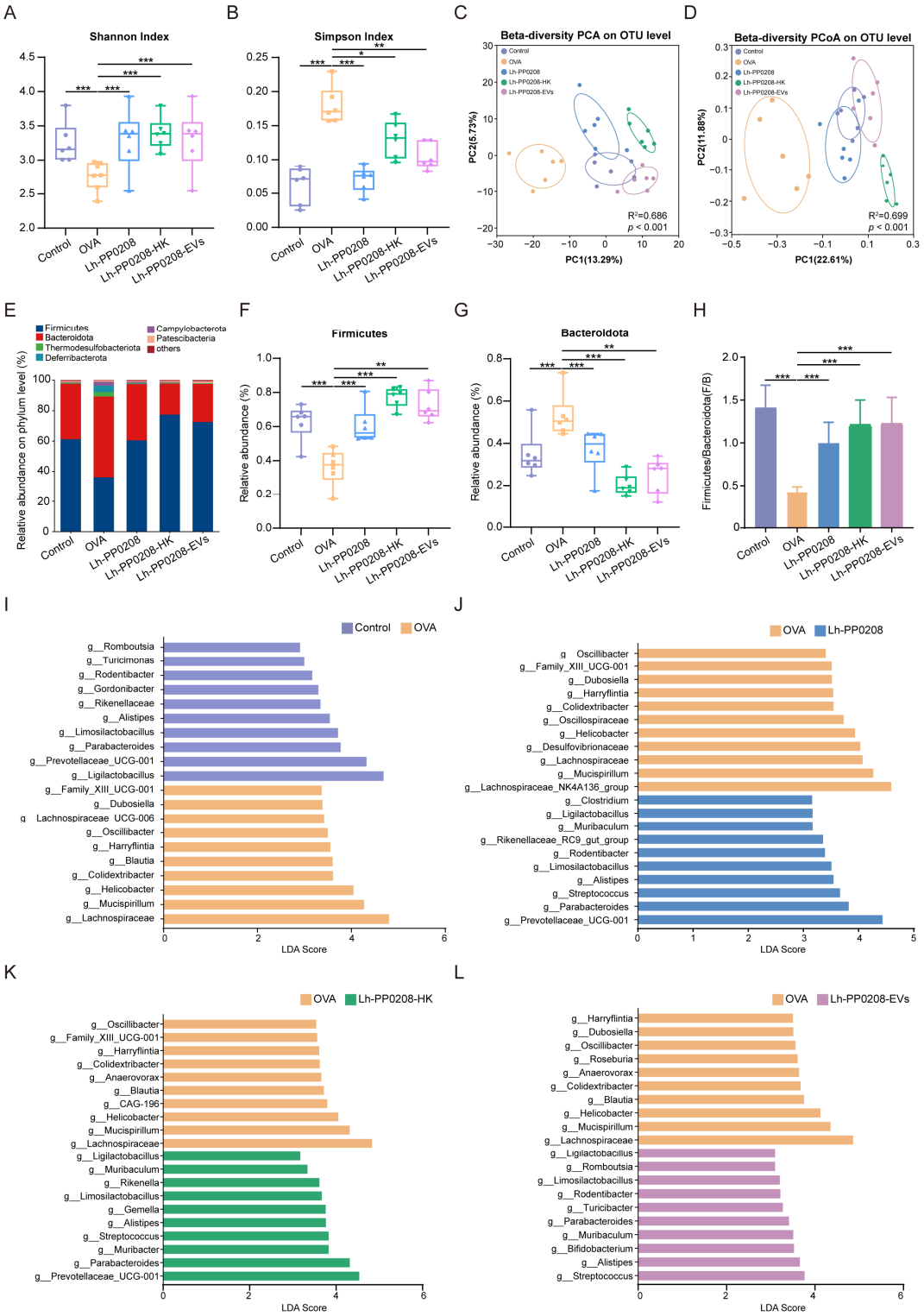

Figure 3. Associated shifts in gut microbiota profiles following *L. helveticus* PP0208 and its derivatives treatment in OVA-challenged AR mice. (**A**,**B**) Alpha diversity evaluated by Shannon (**A**) and Simpson indices (**B**). (**C**,**D**) Beta-diversity analysis based on ASV profiles: PCA (**C**) and PCoA (**D**). (**E**) Relative abundance of the phylum. (**F**,**G**) Relative abundance of *Firmicutes* (**F**) and *Bacteroidota* (**G**). (**H**) The ratio of *Firmicutes* to *Bacteroidota*. (**I**–**L**) Genus-level LEfSe analysis displaying bacterial genera with differential enrichment between groups. LDA score threshold = 3. (**I**) Control vs. OVA group; (**J**) OVA vs. Lh-PP0208 group; (**K**) OVA vs. Lh-PP0208-HK group; (**L**) OVA vs. Lh-PP0208-EVs group. Data are presented as mean ± SEM, $n = 6$/group. * $p < 0.05$, ** $p < 0.01$, *** $p < 0.001$.

At the phylum level, *Firmicutes* and *Bacteroidota* constituted the dominant bacterial taxa across all groups (Figure 3E). Further quantitative analysis revealed that the relative abundance of *Firmicutes* was significantly reduced in the OVA group compared with the Control group ($p < 0.001$), while the relative abundance of *Bacteroidota* was elevated. Following oral administration of Lh-PP0208, Lh-PP0208-HK or Lh-PP0208-EVs, *Bacteroidota* abundance was significantly decreased, while *Firmicutes* abundance partially rebounded toward levels observed in the non-allergic Control group (Figure 3F,G). Consistently, a lower *Firmicutes/Bacteroidota* (F/B) ratio was detected in OVA mice, and this ratio was markedly elevated following all three interventions (Figure 3H).

Subsequently, LEfSe was applied to identify differential taxa enriched in experimental groups. In the OVA group, taxa belonging to *Lachnospirales*, *Mucispirillum* and *Helicobacter* were identified as predominantly enriched taxa. In contrast, the Control group was characterized by high abundance of *Limosilactobacillus*, *Prevotellaceae* and *Ligilactobacillus* (Figure 3I). After Lh-PP0208 intervention, differential taxa mainly included multiple members such as *Prevotellaceae*, *Parabacteroides*, *Limosilactobacillus*, *Ligilactobacillus* and *Streptococcus* (Figure 3J). Lh-PP0208-HK treatment enriched a broad range of *Prevotellaceae*, *Parabacteroides*, *Limosilactobacillus*, *Ligilactobacillus* and *Muribaculum*, while Lh-PP0208-EVs intervention increased the abundance of *Streptococcus*, *Alistipes*, *Limosilactobacillus*, *Ligilactobacillus* and *Bifidobacterium* (Figure 3K,L). Of note, although *Limosilactobacillus* and *Ligilactobacillus* are enriched in intervention groups relative to the OVA group in genus-restricted LEfSe, these two genera are also biomarkers of the non-allergic Control group, indicating their depletion upon OVA-challenged allergic challenge. Their elevated abundance after intervention reflects partial rebounds rather than taxon-specific enrichment exclusively driven by the tested formulations. These data illustrate that Lh-PP0208 and its derivatives were associated with distinct but overlapping alterations in gut microbial composition.

We further constructed microbial co-occurrence networks to characterize interactions across groups (Figure 4A). Network topology exhibited obvious differences among the five experimental groups. In the OVA group, the number of microbial connections was decreased relative to the Control group. Supplementation with Lh-PP0208, Lh-PP0208-HK or Lh-PP0208-EVs was accompanied by a higher total number of network connections, indicating enhanced interactions within the gut microbiota. In addition, substantial shifts in correlation patterns between *Lactobacillus* and other commensal bacteria were observed upon OVA induction; such disturbed network patterns shifted toward control-like configurations following probiotic and EV interventions. The bootstrap stability of the co-occurrence network edges is shown in Figure 4B (B = 500 resamples). Compared with the Control group, the OVA group showed fewer total edges and a lower proportion of highly stable edges, indicating a destabilized microbial network; all three interventions were accompanied by edge counts and stability values shifting toward Control-group levels. Collectively, these findings indicated that Lh-PP0208 and its derivatives were associated with shifts in gut microbiota profiles in AR mice.

2.4. Associations Between Gut Microbiota, Allergic Symptoms and Immune Indicators Following Intervention with L. helveticus PP0208 and Its Derivatives

To further clarify the linkage between gut microbiota and allergic symptoms, we analyzed the relative abundance of gut microbiota and performed correlation analysis. A heatmap displaying the relative abundance of differential genera across all groups was generated (Figure 5A). Violin plots quantified the abundance of microbes (Figure 5B). Consistent with LEfSe results, A2, ASF356, *Lachnoclostridium*, *Anaerotruncus*, *Faecalimonas* and *Oscillibacter* were enriched in the OVA group. Meanwhile, the abundances of several genera depleted in OVA-challenged mice, including *Alistipes*, *Anaeroplasma*, *Butyribacter*, *Odoribacter*,

Roseburia and *Muribaculum*, were higher after all three treatments. *Limosilactobacillus* and *Ligilactobacillus* were enriched in both the Control vs. OVA comparison (Figure 3I) and the OVA vs. intervention comparisons (Figure 3J–L). Distance-based redundancy analysis (db-RDA) was performed to visualize the correlation between gut microbiota composition and allergic indicators (Figure 5C). The distribution of samples indicated clear separation between the OVA and Control groups along the db-RDA1 and db-RDA2 axes. Key allergic indicators, including nose-rubbing frequency, sneezing events, spleen index, IgE and IL-4, were positively correlated with the microbial community characteristics of the OVA group. In contrast, immune tolerance-related parameters such as Treg proportion, IFN-γ and IL-10 were closely associated with the microbiota profile of the Control and intervention groups.

A Spearman correlation heatmap was constructed to quantify pairwise relationships between differential bacterial genera and phenotypic/immune parameters. After controlling for treatment group in partial Spearman analysis, the key associations remained significant ($q < 0.05$). For example, pro-allergic indicators (nose-rubbing, sneezing, spleen index, serum IgE and IL-4) exhibited positive correlations with genera enriched in the OVA group, such as *Mucispirillum* and *Helicobacter*, while showing negative correlations with *Limosilactobacillus*, *Ligilactobacillus* and *Parabacteroides* enriched in the treatment groups. Conversely, anti-inflammatory indicators (Treg percentage, IFN-γ and IL-10) were positively correlated with *Limosilactobacillus*, *Ligilactobacillus* and *Parabacteroides*, while showing negative correlations with *Mucispirillum* and *Helicobacter*. A subset of weaker genus–phenotype links, by contrast, were attenuated, consistent with a portion of the raw correlations reflecting group-level differences rather than direct microbe–host coupling (Figure 5D). The abundance of all relevant bacterial genera is shown in Figure S1. Collectively, *L. helveticus* PP0208 and its derivatives were associated with shifts in the gut microbiota in OVA-challenged mice, and differential gut microbiota genera are closely correlated with allergic symptoms and immune homeostasis markers.

2.5. Fecal Metabolome Alterations and Microbiota–Metabolite Associations Linked to L. helveticus PP0208-Derived Interventions

To characterize the alterations of gut metabolites associated with Lh-PP0208 interventions, untargeted metabolomics analysis of feces was performed. PCA demonstrated obvious separation of metabolic profiles between the Control and OVA groups, indicating that OVA allergic challenge induced profound shifts in the gut metabolome (Figure 6A). Permutation testing ($n = 1000$ permutations) confirmed model validity, with $R^2Y = 0.65$ and $Q^2 = 0.72$ for the original model. The intercepts of the permuted models were $R^2 = 0.2151$ and $Q^2 = -0.2403$; the negative Q^2 intercept indicates no overfitting. (Permutation $p < 0.05$; Figure 6B). KEGG classification illustrated differential metabolites were assigned to metabolic pathways, followed by human disease and environmental information processing categories (Figure 6C). Compared with the OVA group, the Control group exhibited 323 upregulated and 277 downregulated metabolites. Intervention with Lh-PP0208 and its derivatives led to distinct sets of differentially abundant metabolites (Figure 6D,E). Lh-PP0208 treatment yielded 359 elevated and 141 reduced metabolites; Lh-PP0208-HK yielded 92 increased and 810 decreased metabolites; Lh-PP0208-EVs treatment resulted in 119 upregulated and 385 downregulated metabolites.

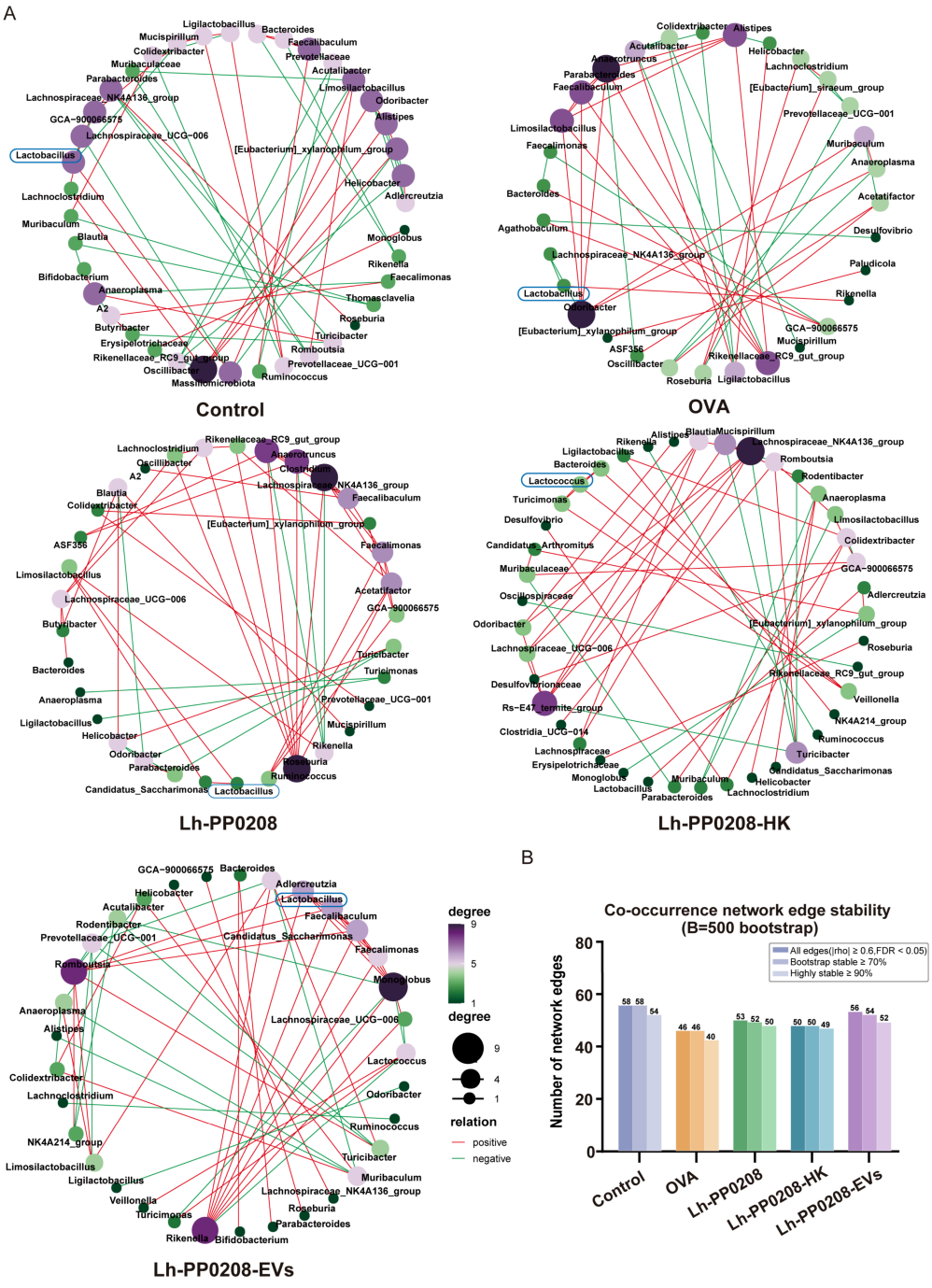

Figure 4. Alterations in gut-microbial co-occurrence networks in OVA-challenged AR mice following *L. helveticus* PP0208 and its derivatives treatment. (**A**) Genus-level microbial co-occurrence networks of the Control, OVA, Lh-PP0208, Lh-PP0208-HK and Lh-PP0208-EVs groups. Nodes represent bacterial genera, node size indicates degree, red lines denote positive correlations, and green lines represent negative correlations. The genus *Lactobacillus* is highlighted with blue circles. (**B**) Co-occurrence networks were inferred at the genus level using SPIEC-EASI with Meinshausen–Bühlmann neighborhood selection. Edges were retained when |Spearman ρ| ≥ 0.6 and BH-FDR $q < 0.05$. Bootstrap stability (B = 500) was assessed by resampling samples with replacement; bars show total edges (dark), edges stable in ≥70% of bootstrap iterations (medium), and edges stable in ≥90% (light). Mean edge stability across all groups exceeded 97%, indicating robust network structure despite limited sample size.

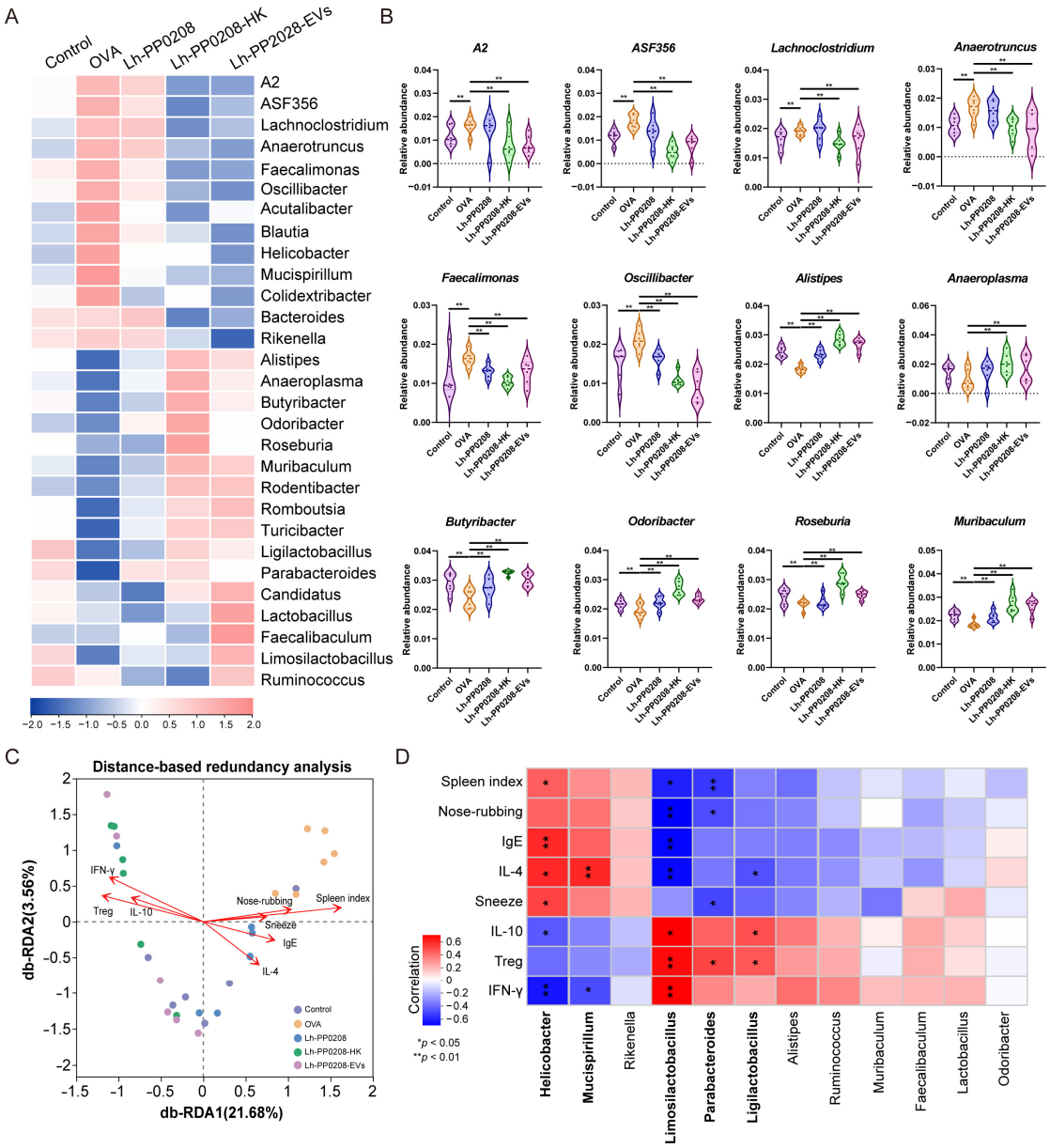

Figure 5. Associations between gut microbiota, allergic symptoms and immune indicators following intervention with *L. helveticus* PP0208 and its derivatives. (**A**) Heatmap illustrating the relative abundance of altered gut bacterial genera across all experimental groups. (**B**) Violin plots showing quantitative comparisons of relative abundance for differential bacterial genera. (**C**) Biplot of db-RDA revealing the correlation between key gut bacterial taxa and allergic phenotypic indicators. (**D**) Partial Spearman analysis heatmap displaying the associations between differential gut bacterial genera and allergic disease-related parameters (spleen index, behavioral symptoms, serum cytokines and IgE). Spearman rank correlation analysis with Benjamini–Hochberg FDR correction for multiple testing. Red represents positive correlation, and blue indicates negative correlation. $q < 0.05$ was considered statistically significant. Data are presented as mean ± SEM, $n = 6$/group. * $p < 0.05$ ** $p < 0.01$.

Top altered metabolites were displayed via bar plots based on $\log_2$(fold change) (Figure 7A–C). Several annotated metabolites, including xanthurenic acid, L-Dopa, ascorbic acid and succinic acid-related features, showed altered abundance after Lh-PP0208 and its derivatives intervention. KEGG enrichment analysis revealed the functional pathways in each comparison group (Figure 7D–F). The pathways enriched after Lh-PP0208 supplementation mainly included carbohydrate metabolism. Distinct alterations in flavonoid biosynthesis and amino-acid metabolic pathways were observed following Lh-PP0208-HK

intervention. Lh-PP0208-EVs exposure was linked to changes in SCFA metabolism and propanoate-related metabolic pathways.

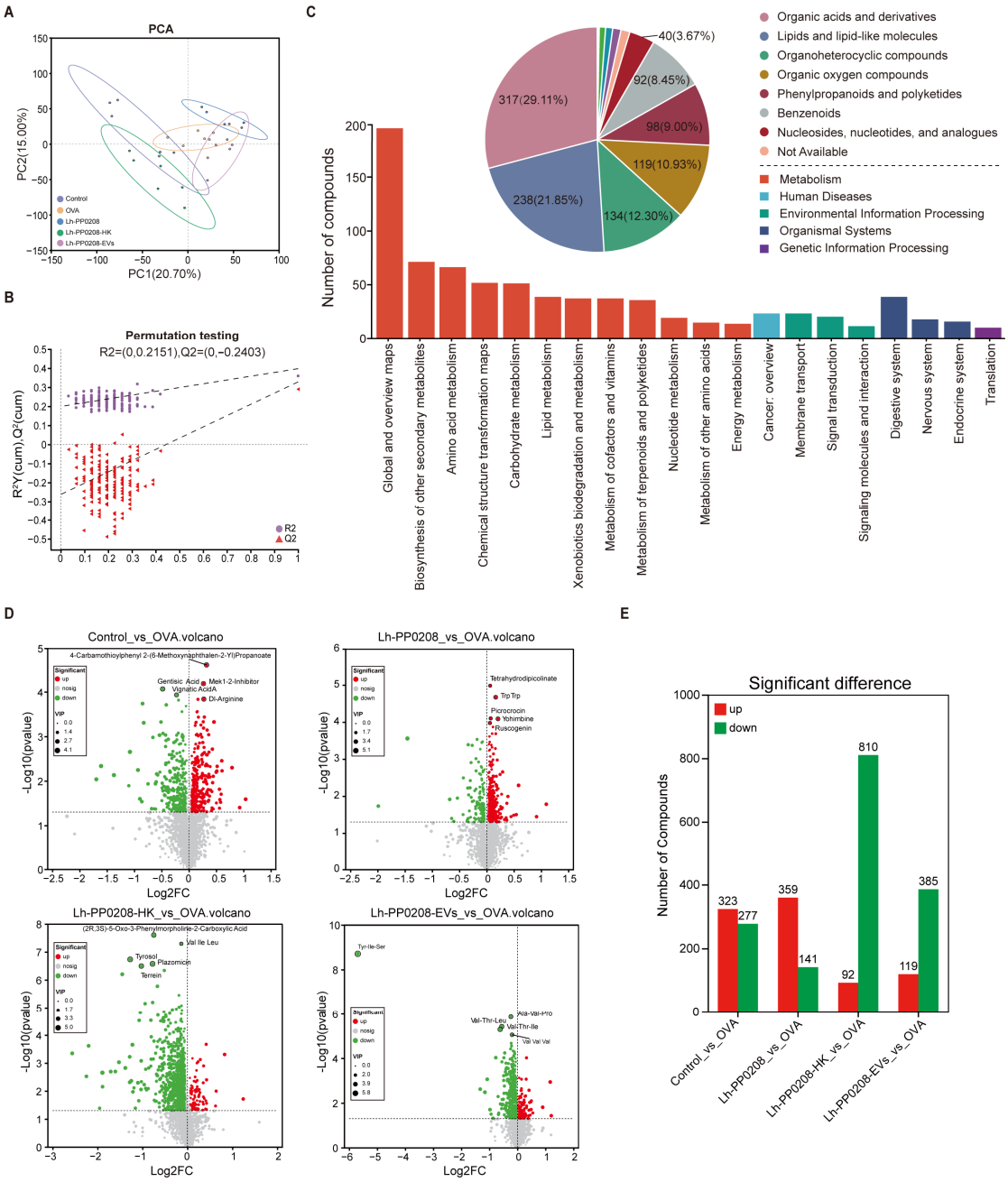

Figure 6. Alterations in fecal gut-metabolome profiles in OVA-challenged AR mice following *L. helveticus* PP0208 and its derivatives treatment. (**A**) PCA score plot displaying the overall separation of the fecal metabolome among all groups. (**B**) Permutation test for the OPLS-DA model to verify model reliability. (**C**) Classification of annotated differential metabolites (pie chart) and enrichment analysis of KEGG metabolic pathways (bar chart). (**D**) Volcano plots illustrating differentially abundant metabolites in four pairwise comparison groups (Control vs. OVA, Lh-PP0208 vs. OVA, Lh-PP0208-HK vs. OVA, Lh-PP0208-EVs vs. OVA). Red dots: upregulated metabolites; green dots: downregulated metabolites; gray dots: non-significant metabolites. (**E**) Bar statistics for the numbers of upregulated and downregulated metabolites in each comparison group. Data are presented as mean ± SEM.

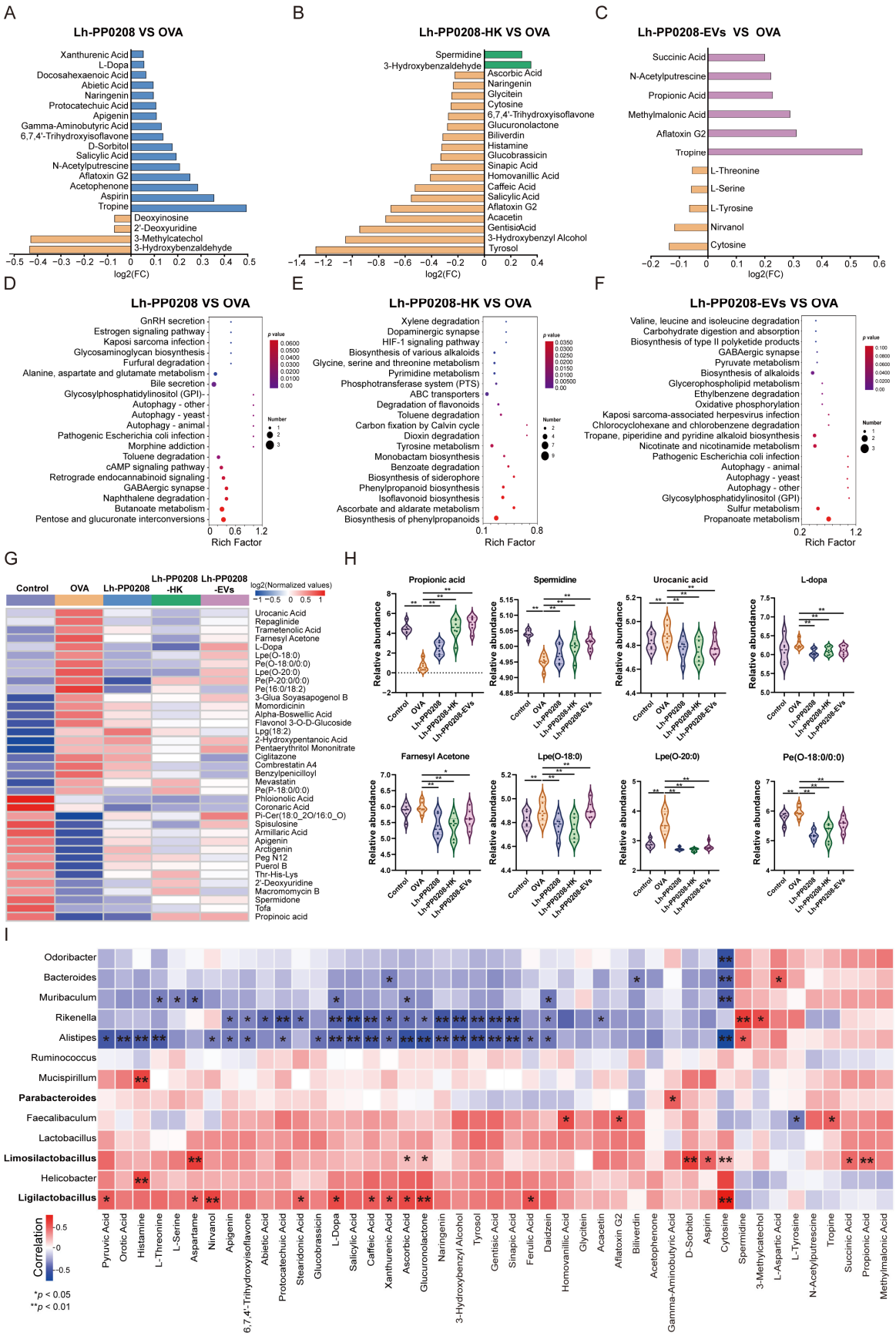

Figure 7. Identification of differential metabolites and metabolic pathways, together with microbiota–metabolite correlation analysis upon treatment with *L. helveticus* PP0208 and its derivatives in OVA-

challenged AR mice. (**A**–**C**) Bar plots showing altered metabolites in pairwise comparisons: Lh-PP0208 vs. OVA (**A**), Lh-PP0208-HK vs. OVA (**B**), Lh-PP0208-EVs vs. OVA (**C**). Red bars represent upregulated metabolites; blue bars represent downregulated metabolites. (**D**–**F**) KEGG pathway enrichment analysis of differential metabolites for each comparison group, visualized by enrichment factor. (**G**) Heatmap displaying relative abundance profiles of representative candidate differential metabolites across all five experimental groups. (**H**) Violin plots showing quantitative comparison of several key characteristic metabolites. * $p < 0.05$, ** $p < 0.01$.(**I**) Correlation heatmap illustrating associations between differential gut bacterial genera and altered metabolites. Spearman correlation analysis with Benjamini–Hochberg FDR correction for multiple testing. Red represents positive correlation, and blue indicates negative correlation. $q < 0.05$ was considered statistically significant. Data are presented as mean ± SEM.

A heatmap summarizes the relative abundance of signature metabolites across all experimental groups (Figure 7G). Violin plots validated the changes in key metabolites such as propionic acid, spermidine and urocanic acid (Figure 7H). We constructed correlation heatmaps to uncover the associations between differential gut bacterial genera and characteristic metabolites (Figure 7I). Collectively, these metabolomic data revealed fecal metabolome alterations and gut microbiota–metabolite associations linked to *L. helveticus* PP0208-related interventions in OVA-challenged AR mice.

3. Discussion

In the present study, a classical OVA-challenged allergic rhinitis (AR) mouse model was established, as evidenced by aggravated nasal allergic symptoms, elevated serum IgE and Th2 pro-inflammatory cytokines, increased inflammatory cell infiltration in BALF, and decreased Treg proportion. Furthermore, OVA sensitization caused obvious mucosal structural damage in nasal, gut and pulmonary tissues, which recapitulated the typical Th2-biased immune response and epithelial barrier dysfunction of clinical AR [17,18]. Under the present experimental conditions, oral administration of *L. helveticus* PP0208 and its derivatives was associated with ameliorated OVA-challenged allergic symptoms. Overall, oral administration of *L. helveticus* PP0208 and its derivatives was associated with ameliorated nasal allergic behavioral symptoms, reduced systemic and local airway inflammation, downregulated IgE/IL-4-associated Th2 inflammatory features, and decreased inflammatory cell infiltration in respiratory tissues. Meanwhile, the interventions increased splenic Treg proportions, attenuated nasal and pulmonary mucosal structural damage, and preserved barrier-associated features. These phenotypic improvements were accompanied by concurrent alterations in gut microbiota and metabolomic profiles following intervention.

Numerous probiotic strains have been verified to alleviate allergic inflammation by regulating gut microbiota and immune tolerance. For example, *L. paracasei* NCC2461 and *L. rhamnosus* Lcr35 attenuate airway allergic inflammation by regulating TLR signaling and Treg differentiation [19,20]. In addition, *Clostridium butyricum* can reverse Th1/Th2 imbalance and inhibit allergic inflammatory progression in different allergic models [21–23]. Consistent with previous studies, our results extended previous observations supporting the immunomodulatory potential and anti-allergic associations of probiotics, and further supplemented the functional characteristics of *L. helveticus* PP0208 and its derivatives in AR intervention, although the precise bioactive components require further investigation.

Accumulating evidence has demonstrated that gut microbiota and metabolites serve as critical modulators of host immune homeostasis, representing promising therapeutic targets for allergic diseases [12]. 16S rRNA gene amplicon sequencing was further performed to explore the gut microbial features associated with the anti-allergic effect of *L. helveticus* PP0208 and its derivatives. The results revealed that OVA sensitization induced significant gut microbial dysbiosis, accompanied by decreased microbial α diversity and

disrupted microbial community structure. Consistent with previous AR studies [24,25], OVA model mice exhibited altered abundance of *Firmicutes* and *Bacteroidota*. Although the *Firmicutes/Bacteroidota* ratio is generally regarded as a key indicator of gut dysbiosis, its variation pattern varies significantly in different allergic models due to distinct allergens and immune response mechanisms [26], suggesting that a causal relationship between this ratio and allergic inflammation requires further verification. Nevertheless, targeted regulation of gut microbial composition to enrich bacteria associated with improved phenotype and deplete pro-inflammatory taxa is confirmed as a strategy for improving allergic diseases [27].

Notably, we identified a stable and consistent pro-inflammatory dysbiosis signature in the OVA group, with *Mucispirillum* significantly enriched at all taxonomic levels. *Mucispirillum* is a genus of bacteria that is widely correlated with intestinal inflammation and has been indicated to influence the intestinal barrier's integrity and function [28]. In contrast, beneficial microbiota represented by *Muribaculaceae*, which are responsible for polysaccharide degradation and short-chain fatty acid (SCFA) production, were markedly depleted in the AR model [29]. Importantly, *L. helveticus* PP0208 and its derivatives were all associated with shifts away from OVA-challenged gut microbial alterations under the experimental conditions used in this study. These findings point to microbiota-related alterations linked to the three tested formulations, although their relative efficacy requires further evaluation using dose-normalized experimental designs. Untargeted fecal metabolomics was further applied to characterize metabolic alterations associated with *L. helveticus* PP0208 and its derivatives intervention, providing additional insights into potential metabolic pathways involved in anti-allergic effects [30]. OVA sensitization induced widespread metabolic disorders involving organic acid metabolism, lipid metabolism and aromatic amino acid metabolism, indicating that AR progression is driven by multi-pathway metabolic disorders.

Intervention with live *L. helveticus* PP0208 was associated with alterations in metabolites involved in SCFA metabolism (including propanoate-related signatures), flavonoid metabolism (represented by apigenin-associated metabolites), and aromatic compound metabolism, alongside shifts in histamine and amino acid-derived metabolic profiles. Such shifts in metabolic profiles point to a gut microenvironment associated with reduced pro-inflammatory potential, which aligns with previous reports describing the restoration of endogenous anti-inflammatory metabolic networks during allergic disease intervention [13,14]. Lh-PP0208-HK exerted a distinct metabolic regulatory effect relative to live bacteria. Notably, Lh-PP0208-HK was associated with the most extensive metabolic changes among the three preparations, with a total of 902 differential metabolites (92 upregulated and 810 downregulated). This disparity may stem from inherent differences in biological activity, bioavailability, and structural properties between viable and heat-killed bacterial preparations [15]. In contrast, Lh-PP0208-EVs induced a unique metabolic landscape characterized by enriched pathways linked to energy metabolism and immune homeostasis. It should be noted that enrichment of SCFA-associated pathways only indicates altered pathway activity and does not directly equate to elevated SCFA concentrations; targeted quantitative assays are required to verify SCFA levels. EV treatment was associated with alterations in SCFA-related metabolic pathways, together with higher splenic Treg frequency and blunted Th2-dominant inflammatory responses. Additionally, Lh-PP0208-EVs altered metabolites participating in neuroactive signaling pathways, hinting at a potential crosstalk between bacterial extracellular vesicles and neuroimmune regulation [16].

Integrated microbiota–metabolite correlation analysis further revealed the intrinsic linkage between gut microbiota and metabolites. Genera showing partial rebounds after intervention (including *Limosilactobacillus*) as well as *Parabacteroides* showed positive correlations with SCFA-related and polyphenol-related metabolic features. In contrast,

pro-inflammatory taxa including *Mucispirillum* and *Helicobacter* were closely associated with histamine and pro-inflammatory amino acid metabolites, and such adverse correlation patterns were effectively disrupted after intervention.

One key limitation of this study concerns cage-level confounding for gut microbiota and fecal metabolome data. Mice were grouped by housing to reduce coprophagy-driven probiotic transfer, yet cage pseudoreplication could not be fully eliminated. With three cages per group (4 mice/cage), cage environmental factors may contribute to omics variation alongside the intervention [31]. Although we balanced the omics subset to two mice per cage and adjusted for cage effects in sensitivity analyses, the small number of cages limits our ability to fully separate cage-level noise from treatment effects, which is especially relevant for 16S and metabolomic datasets susceptible to coprophagy and shared bedding. This should be considered when interpreting microbe–phenotype correlations, and follow-up studies with more cages or single housing are needed. In addition, Lh-PP0208, Lh-PP0208-HK and Lh-PP0208-EVs were normalized by different metrics (CFU, TFU and mass), so their anti-allergic effects cannot be directly compared. Moreover, no quantitative colonization or persistence data were collected for the live Lh-PP0208 preparation: fecal or intestinal recovery, survival and engraftment dynamics of the administered strain (e.g., strain-specific qPCR or culture enumeration) were not measured. Accordingly, the phenotypic associations observed in the live-bacteria group cannot be attributed to stable or sustained intestinal colonization, and a transient immune-modulatory effect after oral gavage cannot be excluded. Follow-up studies should monitor strain-level fecal shedding and intestinal persistence. While TEM and NTA validated EV morphology and size, full proteomic profiling is needed to characterize vesicle composition. Moreover, the observed correlations among gut microbes, metabolites and immune markers are not causal, requiring microbiota depletion or FMT experiments for mechanistic validation. Additional design limitations include the absence of a positive control, an EV vehicle control and a heat-killed supernatant control, the use of only one dose for each preparation, and a therapeutic rather than prophylactic intervention schedule. Consequently, residual soluble culture-medium components, non-vesicular proteins, and lipids cannot be formally excluded. Notwithstanding these limitations, the present study provides a coordinated phenotypic, immunological, microbiome and metabolomic characterization of the anti-allergic effects of *L. helveticus* PP0208 and its derivatives in the OVA-challenged AR model.

4. Materials and Methods

4.1. Bacterial Strain and Preparation

L. helveticus PP0208 was previously isolated from yogurt, identified, and preserved by the Department of Microbiology, Harbin Medical University (China General Microbiological Culture Collection Center, CGMCC No. 28753). The strain was cultured in MRS broth at 37 °C under aerobic conditions with shaking at 200 rpm. After two passages, bacterial cells in the logarithmic growth phase were harvested by centrifugation at 4500 *g* for 15 min at 4 °C, washed twice with sterile phosphate-buffered saline (PBS), and resuspended at a concentration of 1×10^9 CFU/mL. For the heat-killed preparation, the bacterial suspension was incubated at 100 °C for 20 min, and inactivation was confirmed by plating on MRS agar.

EVs were extracted with slight modifications based on previous research [32]. Extracellular vesicles (Lh-PP0208-EVs) were isolated from the culture supernatant of *L. helveticus* PP0208. Briefly, 4 L of bacterial culture was centrifuged at 4500 *g* for 15 min at 4 °C. The supernatant was filtered through a 0.45 μm sterile membrane filter to remove residual bacterial cells, and the filtrate was confirmed sterile by plating on MRS agar. The filtrate was then ultracentrifuged at 120,000 *g* for 60 min at 4 °C. The final LhEV pellet was resuspended in PBS and stored at −80 °C until use. EV protein concentration was quantified

using a BCA protein assay kit (Thermo Fisher Scientific, Waltham, MA, USA) according to the manufacturer's instructions. LhEV morphology was examined by TEM (Hitachi High-Technologies Corporation, Tokyo, Japan) following negative staining. Lh-PP0208-EVs particle size distribution and concentration were measured using a ZetaView nanoparticle tracking analysis system (Particle Metrix GmbH, Inning am Ammersee, Germany). System settings included a laser wavelength of 520 nm and a detection temperature maintained at 26.08 °C. Each sample was analyzed in three independent runs. Purity was assessed by (i) TEM morphology confirming a typical cup-shaped/saucer-shaped EV morphology within the expected size range; (ii) NTA showing a particle population with a mean diameter of 223 ± 3 nm (median 190 nm; peak at 155 nm; X10–X90 = 88–399 nm); (iii) absence of viable bacteria confirmed by plating on MRS agar; and (iv) an identically processed, uninoculated MRS-medium control subjected to the same ultracentrifugation protocol, which yielded no detectable particles by TEM and negligible protein by BCA, excluding co-isolated medium-derived contaminants.

4.2. Animal Model and Experimental Design

Female BALB/c mice (5–6 weeks old, 18–22 g) were purchased from Liaoning Changsheng Biotechnology Co., Ltd., Benxi, China (production license SCXK(Liao)2015-0001). Mice were housed under SPF conditions with sterilized food and water ad libitum and were acclimatized for at least one week prior to the experiment. Animals from different experimental groups were housed in separate cages, and cross-group co-housing was not performed. All mice were fed the same commercial standard maintenance chow for rats and mice throughout the experiment. The guaranteed nutritional composition per kg of diet was as follows: crude protein ≥ 180 g, crude fat ≥ 40 g, crude fiber ≤ 50 g, crude ash ≤ 80 g, moisture ≤ 100 g, calcium 10–18 g, phosphorus 6–12 g, with a calcium: phosphorus ratio ranging from 1.2:1 to 1.7:1. All experimental groups received an identical chow diet, which excluded intergroup dietary differences as a confounding factor affecting intestinal inflammation and gut microbiota. All animals had free access to chow and sterile drinking water to eliminate intergroup dietary variation. All animal procedures were approved by the Institutional Animal Care and Use Committee of Harbin Medical University (Approval HMUIRB2025027). For group randomization: after one-week acclimatization, mice were stratified by body weight and randomly assigned to experimental groups using a random number generator; random group allocation was performed by a research technician who did not participate in subsequent outcome assessment. Mice were housed at 4 animals per cage; each experimental group was allocated to three independent cages ($n = 4$ mice per cage, total $n = 12$ mice per group). The sample size was determined based on previous experience with the OVA-challenged AR model and feasibility considerations. The ovalbumin (OVA)-challenged AR model was established as follows [33]. On days 0, 7, 14, and 21, mice were sensitized by intraperitoneal (i.p.) injection of 200 µL of sensitization solution containing 50 µg OVA (grade V; Sigma-Aldrich, St. Louis, MO, USA) and 2 mg aluminum hydroxide adjuvant in sterile saline. The Control group received the same i.p. schedule but with saline containing 2 mg aluminum hydroxide adjuvant without OVA. From day 22 to day 28, mice were challenged daily by intranasal instillation of 10 µL of 1% OVA (w/v in saline) into each nostril. Mice were randomly assigned to five groups ($n = 12$ per group): (i) Control group (alum-only non-allergic control; i.p. saline containing 2 mg aluminum hydroxide adjuvant, without OVA; intranasal saline; oral saline), (ii) OVA model group (OVA i.p. + intranasal OVA + oral saline), (iii) Lh-PP0208 group (OVA + oral live *L. helveticus* PP0208, 1×10^9 CFU in 200 µL saline once daily), (iv) Lh-PP0208-HK group (OVA + oral heat-killed *L. helveticus* PP0208, 1×10^9 TFU (Total Fluorescence Unit [34,35]) in 200 µL saline once daily, at a dose equivalent to 1×10^9 viable cells before heat inactivation),

and (v) Lh-PP0208-EVs group (OVA + oral LhEVs, 1 mg/kg (based on total EV protein content, equal to 7×10^9 particles/kg) in 200 µL saline once daily). All interventions were administered by oral gavage 1 h before the daily intranasal OVA challenge. The experimental timeline is illustrated in Figure 1C with an identical sensitization and challenge protocol applied across all OVA-challenged groups.

Twelve mice were included in each experimental group to ensure sufficient biological replicates for phenotypic and immunological analyses; fecal samples from six randomly selected mice (two mice per cage per group) were used for subsequent sequencing and LC–MS analysis, so that no single cage dominated the omics subset. For phenotypic and immunological measurements ($n = 12$ per group), we additionally fitted linear mixed-effects models with treatment group as a fixed effect and home cage as a random intercept (lme4::lmer in R); the group effects were robust to cage adjustment, and cage-level variance did not materially alter the significance of between-group differences. For the omics subset ($n = 6$ per group, two mice per cage), the limited within-cage sample size precluded reliable random-effect estimation; we therefore performed a sensitivity analysis including cage as a fixed covariate in PERMANOVA and in differential-abundance models, which did not change the direction or significance of the reported findings (Table S3). Pre-defined animal exclusion criteria included: >15% sustained body weight loss relative to baseline, obvious clinical sickness, or failure to develop expected allergic phenotype after OVA sensitization-challenge. No animals met exclusion criteria, and zero deaths or animal exclusions occurred during the whole experimental workflow.

4.3. Assessment of Allergic Symptoms

Immediately after the final intranasal OVA challenge, nasal allergic behavioral symptoms were evaluated by a blinded observer who counted the number of sneezes and nasal-rubbing episodes over a 10 min observation period in a quiet room [36]. Body weight was recorded daily during the challenge phase.

4.4. Sample Collection

Mice were anesthetized by intraperitoneal administration of Avertin (250 mg/kg), followed by euthanasia via cervical dislocation once sufficient anesthetic depth was confirmed; animals were maintained on a regular diet without fasting before sacrifice 24 h after the final challenge. Blood was collected from the retro-orbital sinus, allowed to clot at room temperature for 2 h, and centrifuged at 3000 *g* for 15 min at 4 °C. Serum was stored at −80 °C until analysis. The spleen was excised, weighed, and the spleen index was calculated as spleen weight (mg) divided by body weight (g). Bronchoalveolar lavage fluid (BALF) was collected by cannulating the trachea, instilling 100 µL of ice-cold sterile PBS, gently massaging the thorax for 20 s, and withdrawing the fluid. This procedure was repeated until a total volume of at least 500 µL was recovered. Nasal mucosa, pulmonary, and colon tissues were excised, fixed in 4% paraformaldehyde for 24 h at room temperature, and processed for histopathology. Fresh fecal samples (2–3 pellets per mouse) were collected under sterile conditions on the day of euthanasia, immediately snap-frozen in liquid nitrogen, and stored at −80 °C for 16S rRNA gene amplicon sequencing and metabolomic analysis.

4.5. Immunological Analyses

Serum IL-4, IL-10, IFN-γ and total IgE levels were measured using commercial ELISA kits (IL-4: Elabscience Biotechnology Co., Ltd., Wuhan, China, cat# E-EL-M0043; IL-10: Elabscience Biotechnology Co., Ltd., Wuhan, China, cat# E-EL-M0046; IFN-γ: Elabscience Biotechnology Co., Ltd., Wuhan, China, cat# E-EL-M0048; total IgE: Dakewe Biotech Co., Ltd., Beijing, China, cat# 1218202) according to the manufacturer's instructions. For splenic

T-regulatory cell analysis, single-cell suspensions were prepared from mouse spleen using mouse spleen lymphocyte separation medium (Solarbio, Beijing, China). Erythrocytes were lysed with red blood cell lysis buffer (Biosharp, Hefei, China). Cell pellets were resuspended in BeyoFC™ flow cytometry staining buffer (Beyotime, Shanghai, China). For flow cytometry staining, cells were first incubated with Zombie Green™ Fixable Viability Kit (Dakewe Biotech, Beijing, China) for dead-cell exclusion. Surface markers were stained with APC anti-mouse CD4 and PE anti-mouse CD25 (both Dakewe Biotech, Beijing, China). After surface-marker staining, cells were fixed and permeabilized using the eBioscience Transcription Factor Fixation/Permeabilization Buffer set (Thermo Fisher Scientific, Waltham, MA, USA) according to the manufacturer's instructions for intranuclear FOXP3 staining. Intranuclear FOXP3 was labeled with Brilliant Violet 421™ anti-mouse FOXP3 (Dakewe Biotech, Beijing, China). Fluorescence-minus-one (FMO) controls and isotype-matched antibody controls were included for gating setup. Gating strategy: first, intact lymphocytes were gated in FSC-SSC dot plots; singlets were discriminated; and viable Zombie-Green-negative cells were selected. $CD4^+$ cells were gated, followed by identification of $CD25^+FOXP3^+$ populations within the $CD4^+$ gate to define $CD4^+CD25^+FOXP3^+$ regulatory T cells (Tregs).

Total BALF cell counts were quantified, and differential cell counts were obtained from Wright–Giemsa-stained cytospin preparations. At least 200 cells per slide were counted under light microscopy to determine the percentages of eosinophils, macrophages, and lymphocytes. Cytological counting of BALF cytospin slides was also performed in a blinded fashion.

4.6. Histopathological Examination

Fixed nasal mucosa, pulmonary, and colon tissues were decalcified (nasal tissues only, in EDTA solution for two weeks), dehydrated through graded ethanol, cleared in xylene, embedded in paraffin, and sectioned at 4 μm thickness. For each animal, 3 serial tissue sections were prepared. Due to tissue processing workload and histological section availability, six randomly selected mice per group were used for quantitative histopathological scoring. Serial sections were stained with hematoxylin and eosin (H&E) for general morphology, periodic acid–Schiff (PAS) for goblet cell mucin and mucus quantification, and Giemsa for eosinophil and mast cell identification in nasal mucosa. Stained sections were examined and photographed under light microscopy at 200× and 400× magnification. Histological scores were assessed based on previously published scoring criteria [37]. For nasal mucosa, inflammatory cell infiltration, mucosal edema, goblet-cell hyperplasia, and epithelial damage were each scored from 0 (no lesion) to 3 (severe lesion); total nasal histological score was the sum of individual sub-scores. For pulmonary tissue, peribronchial inflammatory infiltration, alveolar wall thickening, and alveolar structural destruction were scored 0–3 and summed to yield the total pulmonary injury score. For colonic tissue, mucosal thickness was expressed as the ratio of mucosal layer thickness to total intestinal wall thickness. Histopathological evaluation was performed in a blinded fashion: slide identifiers were anonymized before assessment. Two independent investigators performed histological scoring blindly. Intra-class correlation coefficient (ICC) was calculated to evaluate inter-rater reliability of histological scoring. The ICC for the inter-rater reliability of histological scoring was 0.85 (95% CI [0.78–0.91]). At least five non-overlapping representative visual fields were randomly selected and quantified for each tissue section.

4.7. 16S rRNA Gene Amplicon Sequencing

For microbiome analysis, fecal samples from six randomly selected mice per group were subjected to 16S rRNA gene *amplicon* sequencing. Total genomic DNA was extracted from fecal samples using a stool DNA extraction kit (Qiagen, Germantown, MD, USA). The

V3–V4 hypervariable region of the 16S rRNA gene was amplified using universal primers 338F (5′-ACTCCTACGGGAGGCAGCAG-3′) and 806R (5′-GGACTACHVGGGTWTCTAAT-3′) with barcodes. PCR conditions were: initial denaturation at 95 °C for 3 min; 27 cycles of 95 °C for 30 s, 55 °C for 30 s, and 72 °C for 45 s; followed by a final extension at 72 °C for 10 min. PCR products were quantified, pooled, and sequenced on an Illumina MiSeq platform (Majorbio Bio-Pharm Technology Co., Ltd., Shanghai, China).

Raw sequencing data were processed using the Majorbio Cloud Platform. Amplicon sequence variants (ASVs) were generated using the DADA2 algorithm implemented in the Majorbio Cloud Platform after quality filtering and denoising. Rarefaction curves were generated to evaluate sequencing depth adequacy. Alpha diversity was evaluated using the Shannon and Simpson indices. For beta-diversity analysis, principal component analysis (PCA) and principal coordinate analysis (PCoA) based on Bray–Curtis distances were performed. Permutational multivariate analysis of variance (PERMANOVA) was applied to test for overall compositional differences between groups, with R^2 and *p*-values reported. Permutational multivariate dispersion (PERMDISP) was further used to assess homogeneity of group dispersions. Distance-based redundancy analysis (db-RDA) was used to evaluate associations between environmental factors and microbial community structure. Linear discriminant analysis effect size (LEfSe) was applied to identify differentially abundant genera across groups; the analysis was restricted to the genus level, with the LDA score threshold set to >3 and an alpha significance threshold of 0.05. The Benjamini–Hochberg FDR correction was implemented for multiple-testing adjustment; only taxa passing FDR-corrected $p < 0.05$ were retained as differential biomarkers.

For microbial co-occurrence network analysis at the genus level, SPIEC-EASI was applied to infer microbial associations, which is robust to compositional bias inherent in 16S rRNA gene amplicon sequencing data. Genera with prevalence < 30% across all samples were filtered prior to network construction to reduce spurious correlations. Association edges were retained when the absolute association coefficient $|\rho| \geq 0.6$, with Benjamini–Hochberg FDR correction for multiple testing at $q < 0.05$. Bootstrap resampling ($n = 500$ iterations) was performed to evaluate the uncertainty of total edge counts for each group-specific network. Group-level networks were visualized, where node size represented node degree, red edges indicated positive associations, and green edges indicated negative associations.

4.8. Untargeted Metabolomic Profiling

For untargeted metabolomic profiling, fecal samples from six randomly selected mice per group were analyzed with liquid chromatography–mass spectrometry (LC–MS) at Majorbio Bio-Pharm Technology Co., Ltd. Fecal samples were extracted with 400 µL of methanol/water (4:1, *v*/*v*) containing internal standards (L-2-chlorophenylalanine, 0.02 mg/mL). Samples were homogenized by cryogenic milling (−10 °C, 50 Hz, 6 min), sonicated at low temperature (5 °C, 40 kHz, 30 min), held at −20 °C for 30 min, and centrifuged at 13,000 *g* for 15 min at 4 °C. The supernatant was analyzed on a Thermo Exploris 240 UHPLC-MS system (Thermo Fisher Scientific, Waltham, MA, USA). Chromatographic separation was achieved on a Waters ACQUITY UPLC HSS T3 column (100 × 2.1 mm, 1.8 µm, Waters Corporation, Milford, MA, USA) maintained at 40 °C, with a 3 µL injection volume. The mobile phase consisted of (A) water/acetonitrile (95:5, *v*/*v*) containing 0.1% formic acid and (B) acetonitrile/isopropanol/water (47.5:47.5:5, *v*/*v*/*v*) containing 0.1% formic acid. Mass spectra were acquired in both positive and negative ESI modes over m/z 70–1050, with the following source parameters: spray voltage 3400 V (+)/−3000 V (−), sheath gas 60 arb, auxiliary gas 20 arb, heater temperature 350 °C, capillary temperature 320 °C, S-Lens RF level 70, stepped normalized collision energy of 20/40/60 eV, and Full MS and MS^2

resolutions of 60,000 and 15,000, respectively. Pooled QC samples, prepared by mixing equal volumes of all samples, were injected every 5–15 samples throughout the run. Raw data were processed using Progenesis QI v3.0 (Waters Corporation, Milford, MA, USA) for peak picking, alignment, and annotation against HMDB, Metlin, and KEGG databases, with a mass tolerance of 10 ppm.

Metabolite identification confidence was reported according to MSI levels: all annotated compounds were at MSI level 2 (putative annotation based on spectral library matching against KEGG and HMDB, with exact mass tolerance ±5 ppm and retention-time matching; no authentic reference standards were run in parallel). MS/MS peak assignments for representative differential metabolites (xanthurenic acid, L-Dopa, urocanic acid, farnesyl acetone, and succinic acid-related features) are provided in Table S4 and Figure S2. Differential metabolites between groups were identified by combining orthogonal partial least-squares discriminant analysis (OPLS-DA), fold-change (FC), and statistical testing. The OPLS-DA model was validated by permutation testing ($n = 1000$ permutations), with R^2Y and Q^2 values reported in the Results. The screening thresholds for differential metabolites were set as: OPLS-DA variable importance in projection (VIP) ≥ 1.0, $|\log_2(\text{fold-change})| \geq 0.5$, and Benjamini–Hochberg FDR-adjusted q-value < 0.05. KEGG pathway enrichment analysis was performed using annotated differential metabolites. Enrichment significance was assessed using the hypergeometric test with Benjamini–Hochberg FDR correction; pathways with FDR-adjusted $q < 0.05$ and rich factor > 0.1 were reported as significantly enriched.

4.9. Integrated Correlation Analysis

To integrate the multi-omics data, Spearman correlation coefficients were calculated between the relative abundances of differential bacterial genera, the levels of key differential metabolites, and the immune phenotypic parameters (serum cytokines, Treg proportions, BALF cell counts). Correlation heatmaps were constructed to visualize the association network. Due to the cost and technical considerations of multi-omics analyses, six biological samples per group were randomly selected for 16S rRNA gene amplicon sequencing and metabolomic profiling, while the remaining animals were retained for phenotypic and immunological analyses. We clarify that the microbial, metabolomic, and immune measurements integrated in the correlation analyses were obtained from the same animals. Because both microbial abundance and phenotypic parameters differed systematically across treatment groups, raw Spearman correlations could be inflated by group-level confounding. We therefore additionally performed partial Spearman correlation analysis controlling for treatment group (ppcor R package; group entered as a categorical covariate), and only associations that remained significant after group adjustment are reported as robust microbe–phenotype links. Associations that were attenuated or lost after group adjustment are interpreted as group-level co-variation rather than direct microbe–host coupling.

4.10. Statistical Analysis

Data were obtained from biological replicates within the animal experiment. Data are presented as mean ± standard error of the mean (SEM) throughout the manuscript, including all figure legends. For comparison among multiple experimental groups, one-way ANOVA was applied after assessing normality (Shapiro–Wilk test) and homogeneity of variance (Levene's test). When ANOVA assumptions of normality or equal variance were violated, a non-parametric Kruskal–Wallis H test followed by Dunn's multiple-comparisons test was used instead. For one-way ANOVA, the Tukey–Kramer post hoc multiple comparison test was performed for pairwise group-to-group comparisons. Exact *p*-values, effect sizes (partial η^2 for ANOVA) and 95% confidence intervals (95% CI) were reported

where applicable. For multi-omics correlation analyses using Spearman rank correlation, Benjamini–Hochberg false-discovery-rate (FDR) correction was applied to account for multiple testing; correlations with FDR-adjusted $q < 0.05$ were considered statistically significant. The statistical significance threshold was set at raw $p < 0.05$ for univariate comparisons. Mixed-effects models and partial Spearman correlation were performed in R v4.3.1 (R Foundation for Statistical Computing, Vienna, Austria) with the lme4 and ppcor packages. All analyses were conducted using GraphPad Prism v8.2.1, GraphPad Software, Boston, MA, USA and the Majorbio Cloud Platform.

5. Conclusions

In conclusion, the present study provides exploratory, correlative evidence that oral formulations of *L. helveticus* PP0208 and its derivatives are associated with reduced allergic features and coordinated shifts in gut microbiota, fecal metabolome, and immune parameters in OVA-challenged AR mice. These interventions were accompanied by partial shifts away from OVA-challenged gut-microbiota profiles, altered fecal metabolic landscapes, and shifts in Th1/Th2 cytokine balance and splenic Treg proportion. Collectively, these correlative findings provide new insights into the anti-allergic actions of this probiotic and its derivatives linked to gut microbiota and metabolites, and lay a foundation for subsequent mechanistic validation and future translational research for allergic rhinitis.

Supplementary Materials: The following supporting information can be downloaded at: https://www.mdpi.com/article/10.3390/ijms272310592/s1.

Author Contributions: Q.M. performed experiments and drafted the manuscript. M.Y. performed bioinformatic analyses on mouse experiments, statistical analyses and visualization. M.D. commented on the study and revised the paper. C.X. and X.L. performed experiments and analyzed data. Y.F. designed and supervised the study and revised the manuscript. All authors have read and agreed to the published version of the manuscript.

Funding: This research was funded by the 2025 Heilongjiang Province "Double First-Class" Discipline Collaborative Innovation Achievement Project to Yong Fang (LJGXCG2025-P10), Heilongjiang Provincial Health Commission Research Project (20251212060510) to Yong Fang and Natural Science Foundation of Heilongjiang Province Funded Project to Qingtai Meng (BS2025H009).

Institutional Review Board Statement: The animal study protocol was approved by the Animal Ethics and Welfare Committee of Harbin Medical University, Harbin, China (protocol code HMUIRB2025027 and approved on 15 October 2025).

Informed Consent Statement: Not applicable.

Data Availability Statement: The 16S rRNA gene amplicon sequencing and metabolomic data presented in this study have been deposited in the public repository NCBI SRA (accession PRJNA1550772); the data reported in this paper have been deposited in the OMIX, China National Center for Bioinformation/Beijing Institute of Genomics, Chinese Academy of Sciences accessed on 6 December 2029. (https://ngdc.cncb.ac.cn/omix: accession no. OMIX022676).

Conflicts of Interest: The authors declare no conflicts of interest.

References

1. Wang, J.; Zhou, Y.; Zhang, H.; Hu, L.; Liu, J.; Wang, L.; Wang, T.; Zhang, H.; Cong, L.; Wang, Q. Pathogenesis of allergic diseases and implications for therapeutic interventions. *Signal Transduct. Target. Ther.* **2023**, *8*, 138. [CrossRef] [PubMed]
2. Nur Husna, S.M.; Tan, H.T.; Md Shukri, N.; Mohd Ashari, N.S.; Wong, K.K. Allergic Rhinitis: A Clinical and Pathophysiological Overview. *Front. Med.* **2022**, *9*, 874114. [CrossRef] [PubMed]
3. Basu, A.; Ramamoorthi, G.; Albert, G.; Gallen, C.; Beyer, A.; Snyder, C.; Koski, G.; Disis, M.L.; Czerniecki, B.J.; Kodumudi, K. Differentiation and Regulation of T(H) Cells: A Balancing Act for Cancer Immunotherapy. *Front. Immunol.* **2021**, *12*, 669474. [CrossRef] [PubMed]

4. Catamerò, F.; Foti Randazzese, S.; Caimmi, D.; Paoletti, G.; Canonica, G.W.; Heffler, E.; Ledda, A.G.; Del Giacco, S.; Costanzo, G.; Guida, G.; et al. Clinical Evaluation of Allergen Immunotherapy for Allergic Asthma. *Biologics* **2026**, *20*, 624174. [PubMed]
5. Yang, H.J. Action-plan and as-needed therapy in allergic rhinitis. *Clin. Exp. Pediatr.* **2024**, *67*, 267–273. [CrossRef] [PubMed]
6. McDonnell, J.; Weller, K.; Pien, L.C. Safety of Intranasal Steroids: An Updated Perspective. *Curr. Allergy Asthma Rep.* **2020**, *20*, 69. [CrossRef] [PubMed]
7. Zhang, Y.; Lan, F.; Zhang, L. Advances and highlights in allergic rhinitis. *Allergy* **2021**, *76*, 3383–3389. [CrossRef] [PubMed]
8. Zemelka-Wiacek, M.; Agache, I.; Akdis, C.A.; Akdis, M.; Casale, T.B.; Dramburg, S.; Jahnz-Różyk, K.; Kosowska, A.; Matricardi, P.M.; Pfaar, O.; et al. Hot topics in allergen immunotherapy, 2023: Current status and future perspective. *Allergy* **2024**, *79*, 823–842. [CrossRef] [PubMed]
9. Boulangé, C.L.; Neves, A.L.; Chilloux, J.; Nicholson, J.K.; Dumas, M.E. Impact of the gut microbiota on inflammation, obesity, and metabolic disease. *Genome Med.* **2016**, *8*, 42. [CrossRef] [PubMed]
10. Kayama, H.; Okumura, R.; Takeda, K. Interaction Between the Microbiota, Epithelia, and Immune Cells in the Intestine. *Annu. Rev. Immunol.* **2020**, *38*, 23–48. [CrossRef] [PubMed]
11. Arpaia, N.; Campbell, C.; Fan, X.; Dikiy, S.; van der Veeken, J.; deRoos, P.; Liu, H.; Cross, J.R.; Pfeffer, K.; Coffer, P.J.; et al. Metabolites produced by commensal bacteria promote peripheral regulatory T-cell generation. *Nature* **2013**, *504*, 451–455. [CrossRef] [PubMed]
12. Lungaro, L.; Malfa, P.; Manza, F.; Costanzini, A.; Valentini, G.; Squarzanti, D.F.; Viciani, E.; Velichevskaya, A.; Castagnetti, A.; Barbalinardo, M.; et al. Clinical Efficacy of Probiotics for Allergic Rhinitis: Results of an Exploratory Randomized Controlled Trial. *Nutrients* **2024**, *16*, 4173. [CrossRef] [PubMed]
13. Trompette, A.; Gollwitzer, E.S.; Yadava, K.; Sichelstiel, A.K.; Sprenger, N.; Ngom-Bru, C.; Blanchard, C.; Junt, T.; Nicod, L.P.; Harris, N.L.; et al. Gut microbiota metabolism of dietary fiber influences allergic airway disease and hematopoiesis. *Nat. Med.* **2014**, *20*, 159–166. [CrossRef] [PubMed]
14. Lu, C.; Gao, Y.; Dong, S.; Sun, Y.; Sun, M.; Han, X.; Li, B.; Li, C.; Zhang, Y.; Li, M. Efficacy of different probiotic regimens for allergic rhinitis: A network meta-analysis. *Complement. Ther. Clin. Pract.* **2025**, *59*, 101954. [CrossRef] [PubMed]
15. Kim, H.; Lee, H.; Bang, W.Y.; Park, H.; Moon, J.S. Comparison of Viable and Heat-Inactivated Lacticaseibacillus rhamnosusIDCC 3201: Anti-Pathogenic, Anti-Inflammatory, and Microbiota Modulating Effect. *Food Sci. Nutr.* **2026**, *14*, e71780. [CrossRef] [PubMed]
16. Molina-Tijeras, J.A.; Gálvez, J.; Rodríguez-Cabezas, M.E. The Immunomodulatory Properties of Extracellular Vesicles Derived from Probiotics: A Novel Approach for the Management of Gastrointestinal Diseases. *Nutrients* **2019**, *11*, 1038. [CrossRef] [PubMed]
17. Baraniuk, J.N. Pathogenesis of allergic rhinitis. *J. Allergy Clin. Immunol.* **1997**, *99*, S763–S772. [CrossRef] [PubMed]
18. He, Y.; Chen, Y.; Xu, S.; Luo, Y.; Qin, F.; Hu, W. Pathogenesis and Key Cells in Allergic Rhinitis. *Int. Arch. Allergy Immunol.* **2025**, *186*, 418–429. [CrossRef] [PubMed]
19. Schabussova, I.; Hufnagl, K.; Tang, M.L.; Hoflehner, E.; Wagner, A.; Loupal, G.; Nutten, S.; Zuercher, A.; Mercenier, A.; Wiedermann, U. Perinatal maternal administration of Lactobacillus paracasei NCC 2461 prevents allergic inflammation in a mouse model of birch pollen allergy. *PLoS ONE* **2012**, *7*, e40271. [CrossRef] [PubMed]
20. Jang, S.O.; Kim, H.J.; Kim, Y.J.; Kang, M.J.; Kwon, J.W.; Seo, J.H.; Kim, H.Y.; Kim, B.J.; Yu, J.; Hong, S.J. Asthma Prevention by Lactobacillus Rhamnosus in a Mouse Model is Associated With CD4(+)CD25(+)Foxp3(+) T Cells. *Allergy Asthma Immunol. Res.* **2012**, *4*, 150–156. [CrossRef] [PubMed]
21. Zhang, J.; Su, H.; Li, Q.; Wu, H.; Liu, M.; Huang, J.; Zeng, M.; Zheng, Y.; Sun, X. Oral administration of Clostridium butyricum CGMCC0313-1 inhibits β-lactoglobulin-induced intestinal anaphylaxis in a mouse model of food allergy. *Gut Pathog.* **2017**, *9*, 11. [CrossRef] [PubMed]
22. Tang, M.L.; Ponsonby, A.L.; Orsini, F.; Tey, D.; Robinson, M.; Su, E.L.; Licciardi, P.; Burks, W.; Donath, S. Administration of a probiotic with peanut oral immunotherapy: A randomized trial. *J. Allergy Clin. Immunol.* **2015**, *135*, 737–744.e8. [CrossRef] [PubMed]
23. Ekmekciu, I.; von Klitzing, E.; Fiebiger, U.; Neumann, C.; Bacher, P.; Scheffold, A.; Bereswill, S.; Heimesaat, M.M. The Probiotic Compound VSL#3 Modulates Mucosal, Peripheral, and Systemic Immunity Following Murine Broad-Spectrum Antibiotic Treatment. *Front. Cell. Infect. Microbiol.* **2017**, *7*, 167. [CrossRef] [PubMed]
24. Chen, Z.; Xu, Q.; Liu, Y.; Wei, Y.; He, S.; Lin, W.; Wang, Y.; Li, L.; Xu, Y. Vancomycin-induced gut microbiota dysbiosis aggravates allergic rhinitis in mice by altered short-chain fatty acids. *Front. Microbiol.* **2022**, *13*, 1002084. [CrossRef] [PubMed]
25. Chen, Z.; He, S.; Wei, Y.; Liu, Y.; Xu, Q.; Lin, X.; Chen, C.; Lin, W.; Wang, Y.; Li, L.; et al. Fecal and serum metabolomic signatures and gut microbiota characteristics of allergic rhinitis mice model. *Front. Cell. Infect. Microbiol.* **2023**, *13*, 1150043. [CrossRef] [PubMed]
26. Qiao, C.; Bian, S.; Huang, H.; Xiao, H.; Ma, L.; Han, R. Impact of ovalbumin allergy on oral and gut microbiome dynamics in 6-week-old BALB/c mice. *Front. Microbiol.* **2024**, *15*, 1439452. [CrossRef] [PubMed]

27. Stojanov, S.; Berlec, A.; Štrukelj, B. The Influence of Probiotics on the Firmicutes/Bacteroidetes Ratio in the Treatment of Obesity and Inflammatory Bowel disease. *Microorganisms* **2020**, *8*, 1715. [CrossRef] [PubMed]
28. Chen, Y.; Ling, Z.; Wang, X.; Zong, S.; Yang, J.; Zhang, Q.; Zhang, J.; Li, X. The beneficial mechanism of chitosan and chitooligosaccharides in the intestine on different health status. *J. Funct. Foods* **2022**, *97*, 105232. [CrossRef]
29. Lagkouvardos, I.; Lesker, T.R.; Hitch, T.C.A.; Gálvez, E.J.C.; Smit, N.; Neuhaus, K.; Wang, J.; Baines, J.F.; Abt, B.; Stecher, B.; et al. Sequence and cultivation study of Muribaculaceae reveals novel species, host preference, and functional potential of this yet undescribed family. *Microbiome* **2019**, *7*, 28. [CrossRef] [PubMed]
30. Vich Vila, A.; Zhang, J.; Liu, M.; Faber, K.N.; Weersma, R.K. Untargeted faecal metabolomics for the discovery of biomarkers and treatment targets for inflammatory bowel diseases. *Gut* **2024**, *73*, 1909–1920. [CrossRef] [PubMed]
31. Landes, R.D. How cage effects can hurt statistical analyses of completely randomized designs. *Lab. Anim.* **2024**, *58*, 476–480. [CrossRef] [PubMed]
32. Shi, Y.; Meng, L.; Zhang, C.; Zhang, F.; Fang, Y. Extracellular vesicles of Lacticaseibacillus paracasei PC-H1 induce colorectal cancer cells apoptosis via PDK1/AKT/Bcl-2 signaling pathway. *Microbiol. Res.* **2022**, *255*, 126921, Correction in *Microbiol. Res.* **2022**, *259*, 126955. [CrossRef] [PubMed]
33. Liu, R.; Zhang, Y.; Wang, Y.; Huang, Y.; Gao, J.; Tian, X.; Ma, T.; Zhang, T. Anti-inflammatory effect of dictamnine on allergic rhinitis via suppression of the LYN kinase-mediated molecular signaling pathway during mast cell activation. *Phytother. Res.* **2023**, *37*, 4236–4250. [CrossRef] [PubMed]
34. Snaidr, L.; Mühlhahn, P.; Beimfohr, C.; Kreuzer, C.; Richly, C.; Snaidr, J. Specific cultivation-independent enumeration of viable cells in probiotic products using a combination of fluorescence in situ hybridization and flow cytometry. *Front. Microbiol.* **2024**, *15*, 1410709. [CrossRef] [PubMed]
35. Mondadori, G.; Amoruso, A.; Visciglia, A.; Deusebio, G.; Pinto, D.; Pane, M.; Rinaldi, F. Heat-Treated Probiotics' Role in Counteraction of Skin UVs-Induced Damage In Vitro. *Cosmetics* **2025**, *12*, 121. [CrossRef]
36. Ryu, G.; Bae, J.S.; Kim, J.H.; Kim, E.H.; Chung, Y.J.; Mo, J.H. Sneezing and Rubbing Counts in Allergic Rhinitis Mouse Models Are a Reliable Indicator of Type 2 Immune Response. *Clin. Exp. Otorhinolaryngol.* **2020**, *13*, 308–311. [CrossRef] [PubMed]
37. Liu, L.; Liang, L.; Yang, C.; Zhou, Y.; Chen, Y. Extracellular vesicles of Fusobacterium nucleatum compromise intestinal barrier through targeting RIPK1-mediated cell death pathway. *Gut Microbes* **2021**, *13*, 1–20. [CrossRef] [PubMed]

Disclaimer/Publisher's Note: The statements, opinions and data contained in all publications are solely those of the individual author(s) and contributor(s) and not of MDPI and/or the editor(s). MDPI and/or the editor(s) disclaim responsibility for any injury to people or property resulting from any ideas, methods, instructions or products referred to in the content.